Title
Nanoscale Measurements of Charge Transfer at Cocatalyst/Semiconductor Interfaces in BiVO4 Particle Photocatalysts

Journal
Nano Letters, 22(23)

ISSN
1530-6984

Authors
Shen, Meikun
Kaufman, Aaron J
Huang, Jiawei
et al.

Publication Date
2022-12-14

DOI
10.1021/acs.nanolett.2c03592

Peer reviewed

NANO LETTERS

pubs.acs.org/NanoLett

Letter

Nanoscale Measurements of Charge Transfer at Cocatalyst/Semiconductor Interfaces in $BiVO_4$ Particle Photocatalysts

Meikun Shen, Aaron J. Kaufman, Jiawei Huang, Celsey Price, and Shannon W. Boettcher*

Cite This: *Nano Lett.* 2022, 22, 9493−9499

Read Online

ACCESS | Metrics & More | Article Recommendations | Supporting Information

ABSTRACT: Semiconductor photocatalyst particles convert solar energy to fuels like H_2. The particles are often assumed to provide crystalline-facet-dependent electron−hole separation. A common strategy is to deposit a hydrogen evolution reaction (HER) electrocatalyst on electron-selective facets and an oxygen evolution reaction (OER) electrocatalyst on hole-selective facets. A precise understanding of how charge-carrier-selective contacts emerge and how they are rationally designed, however, is missing. Using a combination of *ex situ* and *in situ* conducting atomic force microscopy (AFM) experiments and new ionomer/catalyst−semiconductor test structures, we show how heterogeneity in charge-carrier selectivity can be measured at the nanoscale. We discover that the presence of the water/electrolyte interface is critical to induce hole selectivity between the CoO_x water-oxidation catalyst and the $BiVO_4$ light absorber. pH-dependent measurements suggest that negative surface charge on the semiconductor is central to inducing hole selectivity. The work also demonstrates a new approach to control local pH and introduce water using thin-film ionomers compatible with conductive AFM measurements.

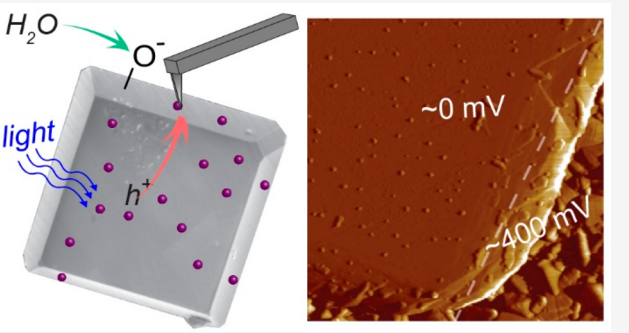

KEYWORDS: *photocatalysis, atomic force microscopy, interface, selectivity, electrocatalyst, semiconductor*

Semiconductor photocatalyst particles have been studied for decades for solar fuel generation, including for H_2 production through water splitting,[1,2] CO_2 reduction,[3,4] and N_2 reduction.[5,6] The solar-to-fuel efficiency of these systems has been low due to some combination of poor carrier mobility, short carrier diffusion lengths, surface recombination, poor carrier selectivity at the interface, and/or poor electrochemical kinetics,[7] although there is no fundamental reason appropriately designed particle photocatalytic systems cannot operate at efficiencies near those of photovoltaics. To suppress competing excited-carrier recombination pathways, a common strategy is to decorate the semiconductor absorbers with electrocatalyst nanoparticles as "cocatalysts".[8,9] It is often reported that different crystal facets of semiconductor particles selectively collect photogenerated electrons or holes due to work-function differences,[1,10−12] and loading HER cocatalysts on electron-selective facets and OER cocatalysts on hole-selective facets has been thought to yield the highest efficiency photocatalysts.[1,10,13] However, the charge-carrier-selective transfer between cocatalysts and semiconductor absorbers is not well understood. The properties of the as-synthesized photocatalysts are diverse, with a large degree of heterogeneity among different particles and the complexity of deposited cocatalysts and their dynamics.[14,15] It has thus been difficult to characterize semiconductor/cocatalyst interfaces in photocatalyst particles and understand what physical and chemical properties are needed to drive a high level of carrier selectivity and thus performance.

Because photocatalyst particles typically operate inside an aqueous electrolyte, the role of the electrolyte must be understood.[16−19] The deposited electrocatalyst nanoparticles are often porous and transform dynamically during catalysis, becoming hydrated (oxy)hydroxides that are redox active.[18,19] Although such dynamic chemical changes are known to be crucial in electrocatalysis,[16,19,20] how the semiconductor−cocatalyst−electrolyte interfaces control charge-carrier selectivity at photocatalyst particles is usually not considered explicitly. Thus, an experimental tool that directly measures the photoresponse at semiconductor−cocatalyst interfaces is useful to isolate and understand the charge-transfer mechanisms on photocatalyst particles.

Herein, we report the use of conductive AFM to directly measure the charge transfer and photoresponse between semiconductor and cocatalyst nanoparticles at single electrocatalyst nanoparticles sitting on larger micron-scale single

Received: September 12, 2022
Revised: November 7, 2022
Published: November 16, 2022

https://doi.org/10.1021/acs.nanolett.2c03592
Nano Lett. 2022, 22, 9493−9499

photocatalyst particles. We study faceted single-crystal $BiVO_4$ semiconductor particles as a model system, as it is a commonly used metal oxide for photocatalysis. We demonstrated nearly ohmic behavior and no electron selectivity on Pt HER cocatalyst nanoparticles, which is contrary to the common assumptions,[1,7,10,13,21,22] and significant hole selectivity on CoO_x OER cocatalyst nanoparticles. Surprisingly, the CoO_x nanoparticles are selective to photogenerated holes only when water exists at the semiconductor−metal interface—the role of water is often not explicitly considered in the design of photocatalysts. Our direct measurements also show facet-selective charge transfer behavior.

We grow $BiVO_4$ microcrystals directly on FTO-coated glass slides to ensure good electrical contact using a modified hydrothermal method.[11] The monoclinic $BiVO_4$ phase is evident from Raman spectroscopy (Figure 1d),[23] and the

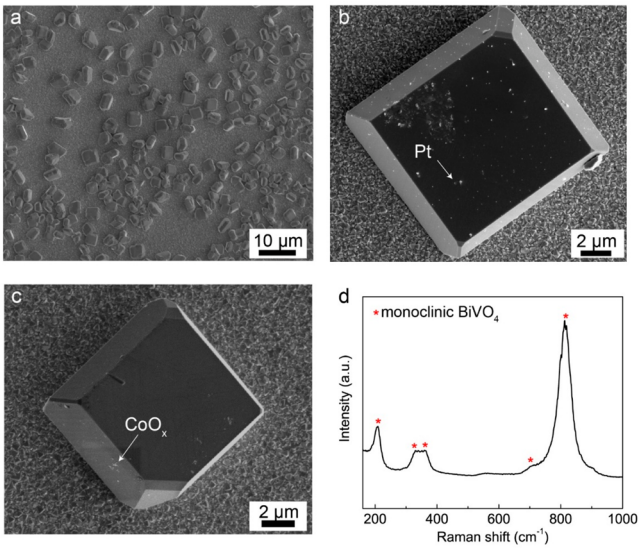

Figure 1. (a) Scanning electron microscopy (SEM) image of the as-synthesized $BiVO_4$ particles on an FTO substrate. (b) Individual Pt-decorated $BiVO_4$ particle. (c) CoO_x-decorated $BiVO_4$ particle. (d) Raman spectra collected on as-synthesized $BiVO_4$ particles. The red stars indicate the characteristic Raman modes of $BiVO_4$.

particles display well-defined platelet morphologies with the (001) facets exposed as the basal plane and the (101) facets as the edge plane.[24] We then decorate the $BiVO_4$ particles with Pt or CoO_x nanoparticles as HER/OER cocatalysts using photoelectrochemical deposition. The nanoparticles are grown on both basal planes and edge planes of the $BiVO_4$ (Figure 1b,c). X-ray photoelectron spectroscopy shows the existence of Pt or Co on the $BiVO_4$ surface with a mixture of Co^{2+} and Co^{3+} (Figure S5).

Figure 2a shows the macroscopic photoelectrochemical behavior of different $BiVO_4$ particles measured in 1.0 M aq. Na_2SO_4 electrolyte (see chopped light data in Figure S1). The large dark current, relative to the light current, in the chopped-light data is due to the low surface coverage of the photoactive particles and the fact that some of the cocatalyst particles also deposit on the underlying FTO substrate (see Figure S3).

The positive photocurrent at 0 V vs E_{OH^-/H_2O} (short circuit) indicates that the cocatalysts selectively collect photogenerated holes, with photogenerated electrons collected by the back substrate contact. The CoO_x-decorated $BiVO_4$ electrodes yield

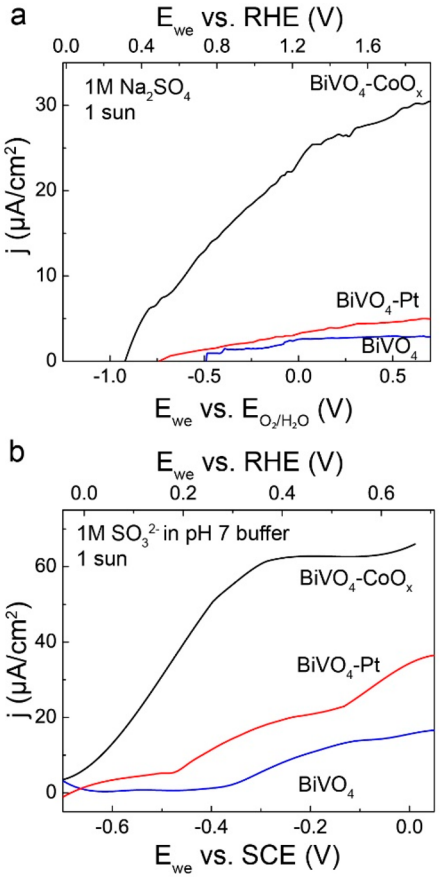

Figure 2. (a) $j_{ph}-V$ curves of different $BiVO_4$ particle electrodes in 1 M Na_2SO_4, under ∼1 sun solar simulation referenced to the reversible potential for OER in this electrolyte and extracted from chopped light data shown in Figure S1. (b) $j_{ph}-V$ curves of different $BiVO_4$ particle electrodes in 1.0 M pH 7 phosphate buffer containing 1.0 M Na_2SO_3 (hole scavenger) under ∼1 sun irradiation.

a larger photovoltage and photocurrent, indicating better hole selectivity at the CoO_x-BiVO_4 interface.[25] CoO_x is also a better water oxidation cocatalyst, with faster kinetics than Pt for the OER.[20,26,27] Although O_2 adsorption from air could modulate the effective work function of Pt nanoparticles and possibly change the selectivity at the $Pt-BiVO_4$ interface, we did not observe a significant change in photochemical behavior of $Pt-BiVO_4$ under N_2 instead of air.

The photoelectrochemical properties of the photocatalysts were then examined in the presence of hole scavengers (1.0 M Na_2SO_3). Contrary to the slow water oxidation reaction, the oxidation of SO_3^{2-} to SO_4^{2-} is kinetically fast. The measured photoresponse is then primarily controlled by the transport to, and collection of photocarriers at, the $BiVO_4$-cocatalyst contact (Figure 2b). Even with the fast hole transfer from the catalyst to the redox-active scavenger, the CoO_x-decorated $BiVO_4$ still has greater photocurrent and photovoltage, showing that the efficiency of the $BiVO_4$ photocatalyst is in large part controlled by the chemical properties of the $BiVO_4$−cocatalyst interface and not solely by bulk generation and recombination in the semiconductor (see chopping data in Figure S2).

To investigate the structure−photoactivity relationship at heterogeneous cocatalyst−$BiVO_4$ interfaces, we used conducting AFM to directly measure the charge transfer properties across single cocatalyst−$BiVO_4$ nanocontacts (see AFM images of different $BiVO_4$ samples in Figure S12). We began

https://doi.org/10.1021/acs.nanolett.2c03592
Nano Lett. 2022, 22, 9493−9499

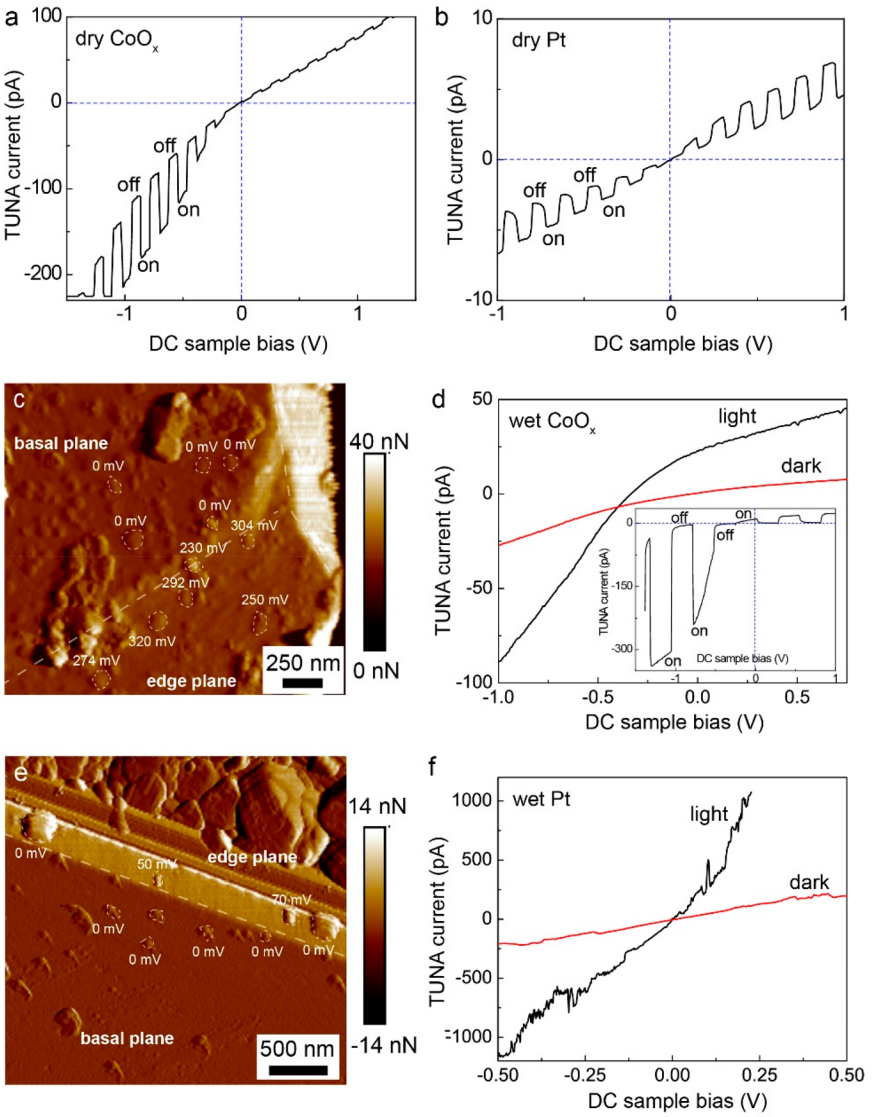

Figure 3. (a) $j-V$ curves of a representative CoO_x-BiVO_4 nanocontact under dry conditions with chopped irradiation. The nanocontacts show rectifying behavior, but no photovoltage is observed. (b) $j-V$ curves of a representative $Pt-BiVO_4$ dry nanocontact under chopped irradiation with ohmic response and no significant photovoltages. (c) Photovoltages collected using conductive atomic force microscopy on CoO_x-decorated $BiVO_4$ particles saturated with water and beneath the ionomer coating. (d) $j-V$ curves of representative CoO_x-BiVO_4 nanocontacts under constant light irradiation. The nanocontacts show rectifying behavior and ~300 mV photovoltage only for CoO_x NPs grown on the basal planes. The inset shows a $j-V$ curve of a representative nanocontact under chopped irradiation. (e) *In situ* photovoltages collected on a Pt-decorated $BiVO_4$ particle saturated with water beneath the ionomer coating. (f) $j-V$ curves of representative $Pt-BiVO_4$ nanocontacts saturated with water under constant illumination and in the dark. The nanocontacts show ohmic behavior, and minimal photovoltages are observed.

with dry *ex situ* measurements. We found in control experiments that the deposited CoO_x nanoparticles form ohmic contacts to the Pt–Ir-coated AFM tip, and the contact resistance between the CoO_x nanoparticles and AFM tip are small compared to the resistance of $BiVO_4$ (see Figure S11).

The CoO_x nanoparticles grown on $BiVO_4$ display rectifying $j-V$ response and the Pt nanoparticles on $BiVO_4$ nearly ohmic behavior. Contrary to the hole selectivity/collection observed in macroscale photoelectrochemical measurements, no significant current was measured across the nanocontacts at short circuit under light irradiation. As positive photocurrents are measured under positive applied bias and negative photocurrents are measured under negative applied bias, the observed photoresponse across the nanocontact is due to the photoconductivity, not selective minority carrier collection (Figure 3a, 3b). Although dry CoO_x-BiVO_4 nanocontacts display slightly asymmetric $j-V$ curves, the selectivity of holes and electrons is apparently insufficient to allow for selective collection, which is likely due to a low barrier height at the interface under dry conditions.

The macroscale photoelectrochemical experiments were performed in electrolyte and the conducting AFM experiments under dry conditions. We hypothesized that water alters the chemical properties of the $BiVO_4$–cocatalyst interface and increases the hole selectivity. To understand the chemical changes at the $BiVO_4$ surface when H_2O is adsorbed, the as-synthesized $BiVO_4$ was annealed at 500 °C to remove surface-bound water. Water-vapor-saturated air was then flown over the $BiVO_4$ film. Infrared absorption spectra of $BiVO_4$ were measured after 20 and 40 min (Figure S4). A sharp absorption peak around 800 cm^{-1}, attributed to a metal–OH stretch, gradually increased, indicating the generation of a surface

https://doi.org/10.1021/acs.nanolett.2c03592
Nano Lett. 2022, 22, 9493–9499

−OH layer when H_2O is adsorbed. Considering the point of zero charge (PZC) of $BiVO_4$ is low (~3.5)[28] and that we measured a zeta potential of the $BiVO_4$ particles in pure H_2O of −27 mV, we expected the $BiVO_4$ surface to be negatively charged in the electrolyte solutions where the photochemical measurements are made.

It is possible that the negatively charged surface layer on $BiVO_4$—induced by the electrolyte—generates increased band bending[29,30] and induces hole selectivity. However, it is difficult to directly measure photocurrents at single-nanoparticle catalyst−semiconductor interfaces to test this hypothesis in an *operando* EC-AFM cell due to background currents.

Here we report a new "ionomer-contact" method to mimic the environment of electrolyte on the electrode; a thin layer (~100 nm thick) of the anion exchange ionomer (sustainion from Dioxide Materials) was spun-coat on the $BiVO_4$ photocatalyst and dried with mild heat (see details in SI). We then saturated the ionomer layer with water before the AFM measurements. The ionomer layer was permeable to water and turned into a soft, gel-like structure that the AFM tip could penetrate to make electrical contact to the Pt or CoO_x cocatalysts. We note that no significant change was observed in macroscopic photoelectrochemical measurements when $BiVO_4$ electrodes were covered with an ionomer (Figure S7). This simple method mimics the wet electrolyte environment and controls the local pH and ionic strength. The technique is straightforward to implement in any conducting AFM instrument and is thus more generally applicable than the specialized EC-AFMs used in the past. The new method enables the direct measurement of $j-V$ response on individual nanocontacts with the presence of water, which is challenging, for example, using an EC-AFM due to the above-mentioned parasitic electrolyte current under full electrolyte submersion of the sample and tip. We first tested this method on the Ni-*n*-Si interface (Figure S6), a well-understood model system studied with EC-AFM.[19] We observed a pinch-off effect on Ni nanoparticles after the ionomer layer was cast and saturated with water (Figures S7 and S8). This is consistent with the idea that the method mimics the electrolyte environment, as the pinch-off could only be detected when NiOOH forms with H_2O present (see details in the SI).

With the $BiVO_4$ particles being saturated with H_2O by the ionomer layer, rectifying behavior is now observed on the CoO_x−$BiVO_4$−H_2O interface (Figure 3d), while the Pt−$BiVO_4$−H_2O interface remains nearly ohmic (Figure 3f). We tried to directly measure the $j-V$ response of a bare $BiVO_4$ surface as well when saturated with H_2O; however, the AFM tip does not make sufficiently good electronic contact with the surface, and we were not able to pass measurable current at reasonable applied biases.

The photovoltage measured at Pt nanocontacts is still small, which is consistent with the macroscopic photoelectrochemical measurements of low photovoltage and photocurrent. The CoO_x nanoparticles grown on the edge planes of $BiVO_4$ particles display an ~300 mV photovoltage (Figure 3c), indicating hole selectivity induced by H_2O and the ionomer. The open-circuit photovoltage was calculated by taking the two-electrode applied voltage from the irradiated $j-V$ curve where the net current was zero. Interestingly, the CoO_x nanoparticles on the basal plane remain nonselective for photogenerated holes (Figure 3c). The different behaviors of CoO_x cocatalysts on different crystal facets provide evidence of facet-dependent charge-carrier separation, which has been long debated due to the conflicting experimental data and lack of a direct characterization method.

We note that Sustainion, like other organic ionomers, will also slowly oxidize under OER potentials.[31] After the short-duration analyses here, the IR spectra of the ionomer film do not display significant differences (Figure S13). The Faradaic efficiency for ionomer oxidation is likely small, contributing minimally to the photocurrent. In the conductive AFM experiments, holes are directly collected by the Pt−Ir-coated tip from the nanoparticle−$BiVO_4$ interface, and the current from electrochemical oxidation of the ionomer is therefore not measured.

To further test our hypothesis, we studied the pH-dependent charge-carrier selectivity on Pt (Figure S5) and CoO_x deposited on $BiVO_4$ photocatalysts (Figure 4a). The macroscale photoelectrochemical measurement shows larger photovoltage and photocurrent in pH = 10 solution compared to pH = 7. The photoresponse becomes small when the pH of the electrolyte was closer to the PZC of $BiVO_4$ (pH = 3.5). We note that the stability of $BiVO_4$ is worse in basic solution, and it is possible that photocorrosion contributes partly to the improved photovoltage in the base. However, the photocurrent measured at short circuit also increased significantly, which definitively indicates better hole collection at the catalyst−$BiVO_4$ interface when electrolyte pH increases, regardless of whether all the holes drive OER or some drive photocorrosion, which is consistent with increased band banding.

The ability to ion-exchange the ionomer thin films allows for nanoscale AFM measurements at different surface-pH microenvironments. The as-prepared cationic ionomer film is balanced with HCO_3^-, which provides a near-neutral local environment. The film was exchanged with 0.1 M KOH solution to mimic a basic electrolyte environment, and we measured the $j-V$ response on the $BiVO_4$−CoO_x−H_2O nanocontact as described before. As in the neutral conditions, only CoO_x nanoparticles grown on the edge plane are selective to photogenerated holes (Figure 4c). Furthermore, the CoO_x nanocontacts display rectifying behavior and a larger photovoltage (~400 mV, presumably due to a higher barrier height) under the locally basic conditions compared to neutral (Figure 4b).

Both the macroscopic measurements and the *in situ* conducting AFM data support the proposed hypothesis. In basic conditions the $BiVO_4$ particles are more negatively charged, as evidenced by its zeta potential (−35 mV at pH = 10 vs −27 mV at pH = 7). Although the water oxidation potential also shifts when the pH of the electrolyte increases, the shift in the band edges appears to be larger than that of the Nernstian OER shift. This surface non-Nernstian process is likely due to nonidealities in proton absorption and surface/near-surface activities with pH, as has been observed for many oxides.[32−34] The more negatively charged layer appears to generate more band bending at the $BiVO_4$ surface, which results in the higher barrier height and larger photovoltage at CoO_x nanocontacts (Figure 4b).

In conclusion, combining new conductive AFM measurements, dry and in the presence of ionomer, with macroscale photoelectrochemical characterization, we developed new insight into the processes which control interface selectivity and charge transfer in semiconductor photocatalyst particles. The underlying interface design principles are complicated. Instead of forming contacts selective to collecting photogenerated electrons, the deposited Pt HER cocatalysts form

https://doi.org/10.1021/acs.nanolett.2c03592
Nano Lett. 2022, 22, 9493−9499

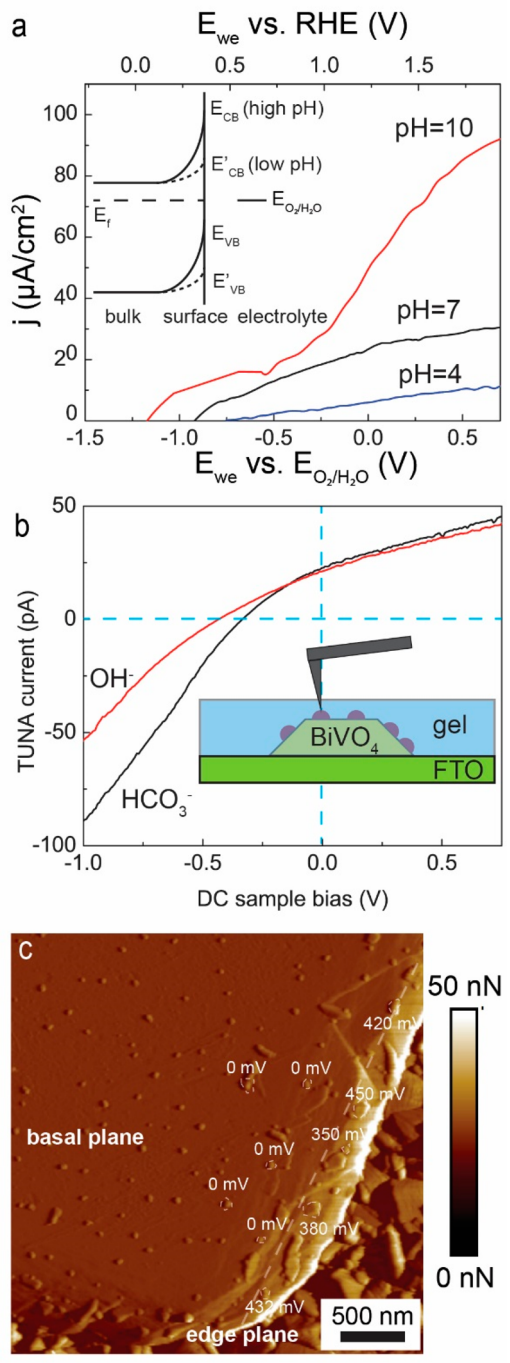

Figure 4. (a) $j-V$ curves of CoO_x–$BiVO_4$ particle electrodes in 1.0 M Na_2SO_4 with different pH under ~1 sun chopped solar simulation. The inset shows the proposed mechanism of surface-charge-induced hole selectivity. (b) $j-V$ curves of representative CoO_x–$BiVO_4$ nanocontacts beneath the ionomer electrolyte layer with and without the exchange of OH^- under illumination. The inset shows a schematic of the conducting-AFM measurement with ionomer coating. (c) Photovoltages collected from a representative CoO_x-decorated $BiVO_4$ particle under a basic ionomer condition; the coating ionomer layer was exchanged with 0.1 M NaOH before the measurement.

near-Ohmic contacts, and other mechanisms are necessary to lead to electron collection on the HER cocatalysts,[35] for example the introduction of a hole-selective catalyst contact nearby. The existence of water and ionomer induces hole selectivity at the CoO_x OER cocatalyst contact on $BiVO_4$. The negative charge layer generated from, likely, deprotonated surface –OH groups appears to increase the band bending to a degree necessary to improve the hole selectivity. The PZC of the semiconductor particle and the pH of the electrolyte thus appear important to consider for different targeted photocatalytic systems. A surface acid/base treatment[36,37] could also be necessary if the surface charge layer is not easy to generate due to the chemical property of the semiconductor absorbers. We also expect a porous, electrolyte permeable cocatalyst (CoO_x, NiO_x) to be of utility, as the surface charge layer could penetrate the cocatalyst and more effectively form an adaptive junction to improve the hole selectivity.[18]

■ ASSOCIATED CONTENT

Supporting Information

The Supporting Information is available free of charge at https://pubs.acs.org/doi/10.1021/acs.nanolett.2c03592.

Additional experimental details on chemicals used in the experiments, characterization of $BiVO_4$, electrode preparation, and sample preparation for conducting AFM. Supporting figures providing raw chopping data of macroscopic photoelectrochemical measurements, IR spectroscopy, XPS spectroscopy, conducting AFM measurements on Ni–Si photoanodes, and dry conducting AFM on $BiVO_4$ particles (PDF)

■ AUTHOR INFORMATION

Corresponding Author

Shannon W. Boettcher – *Department of Chemistry and Biochemistry and the Oregon Center for Electrochemistry, University of Oregon, Eugene, Oregon 97403, United States;* orcid.org/0000-0001-8971-9123; Email: swb@uoregon.edu

Authors

Meikun Shen – *Department of Chemistry and Biochemistry and the Oregon Center for Electrochemistry, University of Oregon, Eugene, Oregon 97403, United States;* orcid.org/0000-0001-8100-4115

Aaron J. Kaufman – *Department of Chemistry and Biochemistry and the Oregon Center for Electrochemistry, University of Oregon, Eugene, Oregon 97403, United States*

Jiawei Huang – *Department of Chemistry and Biochemistry and the Oregon Center for Electrochemistry, University of Oregon, Eugene, Oregon 97403, United States*

Celsey Price – *Department of Chemistry and Biochemistry and the Oregon Center for Electrochemistry, University of Oregon, Eugene, Oregon 97403, United States*

Complete contact information is available at: https://pubs.acs.org/10.1021/acs.nanolett.2c03592

Notes

The authors declare no competing financial interest.

■ ACKNOWLEDGMENTS

This work was funded by the Department of Energy, Basic Energy Sciences award no. DE-SC0014279. M.S. and S.W.B. conceived the experiments and led the project. J.H. collected the Raman and IR spectra. M.S. conducted all other experiments. M.S. and S.W.B. analyzed the data and wrote the manuscript with input from all authors.

REFERENCES

(1) Takata, T.; Jiang, J.; Sakata, Y.; Nakabayashi, M.; Shibata, N.; Nandal, V.; Seki, K.; Hisatomi, T.; Domen, K. Photocatalytic water splitting with a quantum efficiency of almost unity. *Nature* **2020**, *581*, 411−414.

(2) Maeda, K.; Teramura, K.; Masuda, H.; Takata, T.; Saito, N.; Inoue, Y.; Domen, K. Efficient Overall Water Splitting under Visible-Light Irradiation on $(Ga_{1-x}Zn_x)(N_{1-x}O_x)$ Dispersed with Rh-Cr Mixed-Oxide Nanoparticles: Effect of Reaction Conditions on Photocatalytic Activity. *J. Phys. Chem. B* **2006**, *110*, 13107−13112.

(3) Ulmer, U.; Dingle, T.; Duchesne, P. N.; Morris, R. H.; Tavasoli, A.; Wood, T.; Ozin, G. A. Fundamentals and applications of photocatalytic CO_2 methanation. *Nat. Commun.* **2019**, *10*, 3169.

(4) Dhakshinamoorthy, A.; Navalon, S.; Corma, A.; Garcia, H. Photocatalytic CO_2 reduction by TiO_2 and related titanium containing solids. *Energy Environ. Sci.* **2012**, *5*, 9217−9233.

(5) Liu, Q.; Yuan, J.; Gan, Z.; Liu, C.; Li, J.; Liang, Y.; Chen, R. Photocatalytic N_2 Reduction: Uncertainties in the Determination of Ammonia Production. *ACS Sustainable Chem.Eng.* **2021**, *9* (1), 560−568.

(6) Xu, T.; Liang, J.; Li, S.; Xu, Z.; Yue, L.; Li, T.; Luo, Y.; Liu, Q.; Shi, X.; Asiri, A. M.; Yang, C.; Sun, X. Recent Advances in Nonprecious Metal Oxide Electrocatalysts and Photocatalysts for N_2 Reduction Reaction under Ambient Condition. *Small Sci.* **2021**, *1*, 2000069.

(7) Wang, Q.; Domen, K. Particulate Photocatalysts for Light-Driven Water Splitting: Mechanisms, Challenges, and Design Strategies. *Chem. Rev.* **2020**, *120* (2), 919−985.

(8) Hisatomi, T.; Takanabe, K.; Domen, K. Photocatalytic Water-Splitting Reaction from Catalytic and Kinetic Perspectives. *Catal. Lett.* **2015**, *145*, 95−108.

(9) Yang, J.; Wang, D.; Han, H.; Li, C. Roles of Cocatalysts in Photocatalysis and Photoelectrocatalysis. *Acc. Chem. Res.* **2013**, *46* (8), 1900−1909.

(10) Li, R.; Zhang, F.; Wang, D.; Yang, J.; Li, M.; Zhu, J.; Zhou, X.; Han, H.; Li, C. Spatial separation of photogenerated electrons and holes among {010} and {110} crystal facets of $BiVO_4$. *Nat. Commun.* **2013**, *4*, 1432.

(11) Zhu, J.; Fan, F.; Chen, R.; An, H.; Feng, Z.; Li, C. Direct Imaging of Highly Anisotropic Photogenerated Charge Separations on Different Facets of a Single $BiVO_4$ Photocatalyst. *Angew. Chem., Int. Ed.* **2015**, *54*, 9111−9114.

(12) Chen, R.; Pang, S.; An, H.; Zhu, J.; Ye, S.; Gao, Y.; Fan, F.; Li, C. Charge separation via asymmetric illumination in photocatalytic Cu_2O particles. *Nat. Energy.* **2018**, *3*, 655−663.

(13) Li, R.; Han, H.; Zhang, F.; Wang, D.; Li, C. Highly efficient photocatalysts constructed by rational assembly of dual-cocatalysts separately on different facets of $BiVO_4$. *Energy Environ. Sci.* **2014**, *7*, 1369−1376.

(14) Shen, M.; Ding, T.; Rackers, W. H.; Tan, C.; Mahmood, K.; Lew, M. D.; Sadtler, B. Single-Molecule Colocalization of Redox Reactions on Semiconductor Photocatalysts Connects Surface Heterogeneity and Charge-Carrier Separation in Bismuth Oxybromide. *J. Am. Chem. Soc.* **2021**, *143* (30), 11393−11403.

(15) Sambur, J. B.; Chen, T.-Y.; Choudhary, E.; Chen, G.; Nissen, E. J.; Thomas, E. M.; Zou, N.; Chen, P. Sub-particle reaction and photocurrent mapping to optimize catalyst-modified photoanodes. *Nature* **2016**, *530*, 77−80.

(16) Nellist, M. R.; Laskowski, F. A. L.; Lin, F.; Mills, T. J.; Boettcher, S. W. Semiconductor-Electrocatalyst Interfaces: Theory, Experiment, and Applications in Photoelectrochemical Water Splitting. *Acc. Chem. Res.* **2016**, *49* (4), 733−740.

(17) Lin, F.; Bachman, B. F.; Boettcher, S. W. Impact of Electrocatalyst Activity and Ion Permeability on Water-Splitting Photoanodes. *J. Phys. Chem. Lett.* **2015**, *6* (13), 2427−2433.

(18) Lin, F.; Boettcher, S. W. Adaptive semiconductor/electrocatalyst junctions in water-splitting photoanodes. *Nat. Mater.* **2014**, *13*, 81−86.

(19) Laskowski, F. A. L.; Oener, S. Z.; Nellist, M. R.; Gordon, A. M.; Bain, D. C.; Fehrs, J. L.; Boettcher, S. W. Nanoscale semiconductor/catalyst interfaces in photoelectrochemistry. *Nat. Mater.* **2020**, *19*, 69−76.

(20) Trotochaud, L.; Young, S. L.; Ranney, J. K.; Boettcher, S. W. Nickel-Iron Oxyhydroxide Oxygen-Evolution Electrocatalysts: The Role of Intentional and Incidental Iron Incorporation. *J. Am. Chem. Soc.* **2014**, *136* (18), 6744−6753.

(21) Wenderich, K.; Mul, G. Methods, Mechanism, and Applications of Photodeposition in Photocatalysis: A Review. *Chem. Rev.* **2016**, *116* (23), 14587−14619.

(22) Osterloh, F. E. Inorganic nanostructures for photoelectrochemical and photocatalytic water splitting. *Chem. Soc. Rev.* **2013**, *42* (6), 2294−2320.

(23) Frost, R. L.; Henry, D. A.; Weier, M. L.; Martens, W. Raman spectroscopy of three polymorphs of BiVO4: clinobisvanite, dreyerite and pucherite, with comparisons to $(VO_4)^{3-}$ bearing minerals: namibite, pottsite and schumacherite. *J. Raman Spectrosc.* **2006**, *37*, 722−732.

(24) Zhu, W.; Shen, M.; Fan, G.; Yang, A.; Meyer, J. R.; Ou, Y.; Yin, B.; Fortner, J.; Foston, M.; Li, Z.; Zou, Z.; Sadtler, B. Facet-Dependent Enhancement in the Activity of Bismuth Vanadate Microcrystals for the Photocatalytic Conversion of Methane to Methanol. *ACS Appl. Nano Mater.* **2018**, *1*, 6683−6691.

(25) Roe, E. T.; Egelhofer, K. E.; Lonergan, M. C. Limits of Contact Selectivity/Recombination on the Open-Circuit Voltage of a Photovoltaic. *ACS Appl. Energy Mater.* **2018**, *1* (3), 1037−1046.

(26) Burke, M. S.; Kast, M. G.; Trotochaud, L.; Smith, A. M.; Boettcher, S. W. Cobalt-Iron (Oxy)hydroxide Oxygen Evolution Electrocatalysts: The Role of Structure and Composition on Activity, Stability, and Mechanism. *J. Am. Chem. Soc.* **2015**, *137* (10), 3638−3648.

(27) Burke, M. S.; Enman, L. J.; Batchellor, A. S.; Zou, S.; Boettcher, S. W. Oxygen Evolution Reaction Electrocatalysis on Transition Metal Oxides and (Oxy)hydroxides: Activity Trends and Design Principles. *Chem. Mater.* **2015**, *27* (22), 7549−7558.

(28) Heckel, S.; Simmchen, J. Photocatalytic $BiVO_4$ Microswimmers with Bimodal Swimming Strategies. *Advanced Intelligent Systems* **2019**, *1*, 1900093.

(29) Matsumoto, Y.; Yoshikawa, T.; Sato, E. i. Dependence of the Band Bending of the Oxide Semiconductors on pH. *J. Electrochem. Soc.* **1989**, *136*, 1389−1391.

(30) Matsumoto, Y.; Sugiyama, K.; Sato, E. i. Photocathodic Hydrogen Evolution Reactions at p-Type $CaFe_2O_4$ Electrodes with Fermi Level Pinning. *J. Electrochem. Soc.* **1988**, *135*, 98−104.

(31) Krivina, R. A.; Lindquist, G. A.; Yang, M. C.; Cook, A. K.; Hendon, C. H.; Motz, A. R.; Capuano, C.; Ayers, K. E.; Hutchison, J. E.; Boettcher, S. W. Three-Electrode Study of Electrochemical Ionomer Degradation Relevant to Anion-Exchange-Membrane Water Electrolyzers. *ACS Appl. Mater. Interfaces* **2022**, *14* (16), 18261−18274.

(32) Lyon, L. A.; Hupp, J. T. Energetics of the Nanocrystalline Titanium Dioxide/Aqueous Solution Interface: Approximate Conduction Band Edge Variations between $H_0 = -10$ and $H_- = +26$. *J. Phys. Chem. B* **1999**, *103* (22), 4623−4628.

(33) Trzesniewski, B. J.; Digdaya, I. A.; Nagaki, T.; Ravishankar, S.; Herraiz-Cardona, I.; Vermaas, D. A.; Longo, A.; Gimenez, S.; Smith, W. A. Near-complete suppression of surface losses and total internal quantum efficiency in $BiVO_4$ photoanodes. *Energy Environ. Sci.* **2017**, *10*, 1517−1529.

(34) Du, C.; Zhang, M.; Jang, J.-W.; Liu, Y.; Liu, G.-Y.; Wang, D. Observation and Alteration of Surface States of Hematite Photoelectrodes. *J. Phys. Chem. C* **2014**, *118* (30), 17054−17059.

(35) Kaufman, A. J.; Krivina, R. A.; Shen, M.; Boettcher, S. W. Controlling Catalyst-Semiconductor Contacts: Interfacial Charge Separation in p-InP Photocathodes. *ACS Energy Lett.* **2022**, *7* (1), 541−549.

https://doi.org/10.1021/acs.nanolett.2c03592
Nano Lett. 2022, 22, 9493−9499

(36) Fang, S. M.; Chen, B. H.; White, J. M. Photoassisted water-gas shift reaction on platinized titania. The influence of preparation parameters. *J. Phys. Chem.* **1982**, *86* (16), 3126−3130.
(37) Wagner, F. T.; Somorjai, G. A. Photocatalytic and photoelectrochemical hydrogen production on strontium titanate single crystals. *J. Am. Chem. Soc.* **1980**, *102* (17), 5494−5502.

https://doi.org/10.1021/acs.nanolett.2c03592
Nano Lett. 2022, 22, 9493−9499